

Towards the First Continuous Wave Compatible Multistage Depressed Collector Design for High Power Gyrotrons

Benjamin Ell, Chuanren Wu, Gerd Gantenbein, Stefan Illy, Moritz Misko, Ioannis Gr. Pagonakis, Jörg Weggen, Manfred Thumm, *Fellow, IEEE*, and John Jelonnek, *Senior Member, IEEE*

Abstract—The Multistage Depressed Collector (MDC) is essential to significantly increase the overall efficiency of the gyrotron. To date, a Short Pulse (SP) MDC prototype system has been manufactured and is currently under test. The long-term goal that makes the most sense is to use MDCs on 2-MW fusion gyrotrons in Continuous Wave (CW) operation. To achieve this, a CW MDC system based on the same physical principle as the SP system is designed and analyzed for the first time. The highlights of this design are the sweeping systems to keep the thermal loading within an acceptable limit when the MDC is operated in CW. In the present analysis, the expected performance and size of the new CW MDC design is compared with that of the SP MDC prototype and with the corresponding Single-stage Depressed Collectors (SDC) as a reference. In addition, the effects of thermal expansion in CW operation are analyzed and discussed.

Index Terms—Electron beams, Gyrotrons

I. INTRODUCTION

MDC technology is one of the key components for high power CW gyrotrons with output powers of 2 MW and above. An MDC can significantly increase the efficiency of a vacuum electron device and distribute the power loading onto multiple stages. The increase in efficiency is possible due to multiple deceleration potentials, which separate the spent beam electrons based on their initial kinetic energy. The single deceleration potential of an SDC is limited to the initial kinetic energy of the slowest spent beam electron. Higher deceleration

potentials would cause reflections of slow spent beam electrons to the cavity and could influence the interaction with the radio frequency (RF) wave. The potentials of an MDC can be adjusted according to the widely spread energy distribution of the spent electron beam for an optimized collector efficiency. Only the potential of the first stage is limited by the slowest electron.

The efficiency of the collector is defined as the ratio of the recovered power P_r to the initial power P_i of the spent beam, i.e. $\eta_{col} = P_r/P_i$ and is typically in a range of 50 % to 60 % for a conventional SDC in a high power gyrotron [1-3]. Another advantage of the flexibility of the deceleration potentials of an MDC is the possibility to optimize the collector system towards a smaller size or an optimized power loading distribution. The total generated thermal power for an SDC is significantly higher than for an MDC in the same gyrotron. A higher thermal power correlates directly with a larger required surface area where the electron beam is collected, due to the limitations of current cooling techniques.

The most promising concept for spent electron beam separation for a gyrotron MDC is the $E \times B$ drift principle [4,5] with perpendicular electric and magnetic fields to achieve a radial drift of the spent beam electrons [6-8]. An axial magnetic field in combination with an azimuthal electric field [4], or an azimuthal magnetic field in combination with an axial electric field [9] are required to achieve the desired field profiles. A systematic investigation of high power gyrotron collector systems with high efficiencies is ongoing at KIT [5,10-16].

In this work, the concept of an azimuthal electric field is deployed for all MDC designs and is generated out of three helical and three straight cuts, separating the first and second stage. The first stage is at the bottom of the collector and the second stage at the top with a cylindrical top section for all MDC designs. The $E \times B$ region is defined as the region where both stages overlap in axial direction and an azimuthal electric field is created. The drift principle and field components in the center of the $E \times B$ region of a simplified geometry, without helical extensions, is shown in Fig. 1 on the left side. Though the sectors with clockwise E_ϕ are unwanted, they are unavoidable due to Faraday's law. Fortunately, these sectors can be kept small in the designs. The majority of the spent beam electrons is influenced by the counterclockwise E_ϕ in the larger part of the cross-section and is accelerated by a radial drift to the outside. The slow electrons are collected on the helical surface of the first stage due to the electron drift. The guiding

Manuscript received [month] [day], [year]; revised [month] [day], [year]; accepted [month] [day], [year]. Date of publication [month] [day], [year]; date of current version [month] [day], [year]. Part of this work has been carried out within the framework of the EUROfusion Consortium, funded by the European Union via the Euratom Research and Training Programme (Grant Agreement No 101052200 — EUROfusion). Views and opinions expressed are however those of the author(s) only and do not necessarily reflect those of the European Union or the European Commission. Neither the European Union nor the European Commission can be held responsible for them. The review of this paper was arranged by Editor [Name]. (Corresponding author: Benjamin Ell.)

The authors are with the Institute for Pulsed Power and Microwave Technology, Karlsruhe Institute of Technology, 76131 Karlsruhe, Germany (e-mail: Benjamin.Ell@kit.edu; John.Jelonnek@kit.edu).

Color versions of one or more of the figures in this paper are available online at <http://ieeexplore.ieee.org>.

Digital Object Identifier xxxxxxxxxxxxxxxx

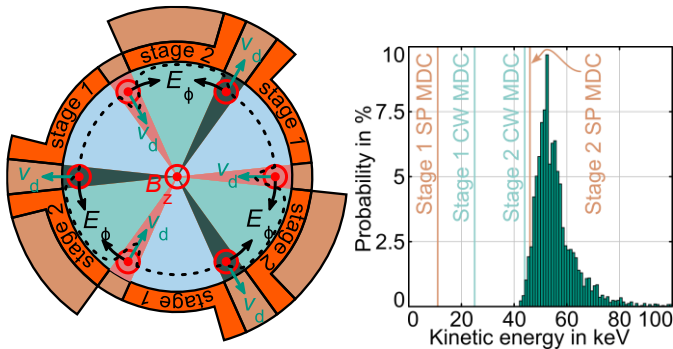


Fig. 1: A representative cross-section showing the principle in the center of the $E \times B$ region of a simplified MDC design (left) and the energy spectrum of the spent electron beam (right).

center radius of the faster electrons is only slightly influenced by the $E \times B$ drift before the collection on the second stage.

Few details of the SP MDC prototype are presented in Sec. II, while the design approach of the CW MDC is presented in Sec. III. The steps required to reduce the power loading density and possibilities for sweeping systems for a CW MDC are presented in Sec. IV. Finally, the results of the thermal expansion investigation of the CW MDC are briefly discussed in Sec. V.

II. SHORT PULSE COLLECTORS

The SP MDC prototype is optimized for the spent electron beam energy distribution, shown in Fig. 1 on the right side, of the KIT 170 GHz, 2 MW coaxial cavity gyrotron [17] with -11 kV and -46 kV depression potential on the first and second stage, respectively. These potentials were chosen for a theoretical optimal collector efficiency of at least 80 % and a high potential difference between both stages to achieve a

strong $E \times B$ drift in a compact design. The design of the SP MDC collector is presented in more detail in Ref. 13 to 16.

A size comparison between the SP SDC (used for the operation of the same gyrotron [17]) and MDC is shown in Fig. 2 (left side and middle) including some of the key dimensions. A photo of the manufactured SP MDC prototype is shown on the right side of Fig. 2. The overall MDC system is larger than the SDC. However, the sizes of the copper electrodes are very comparable with a smaller inner radius and an increased length for the MDC. It should be also mentioned that the size of the MDC could be significantly decreased with a conical bottom section of the first stages to match the diverging magnetic field lines of the gyrotron magnet. The complexity of production would be increased, and the flexibility of the system decreased with such a conical section. Another possibility to reduce the length of the MDC would be to use a different gyrotron magnet with a faster diverging magnetic field. However, this would also require a different gyrotron. The length of the SDC, on the other hand, is independent of the magnetic field profile used.

The main limitation in the maximum pulse length of such SP collectors is the fast-increasing inner surface temperatures at the collector stages due to a high localized power loading density. The typical wall thickness of a high power gyrotron collector is in the range of 10-20 mm. The temperature at the outer surface of the collector is not influenced during SP operation due to significantly slower thermal wave propagation in the material [18]. The main purpose of an improved cooling system of a SP collector is an increase in the pulse repetition rate. The critical temperature at the inner collector wall is not significantly influenced by an improved cooling system.

The power loading density on the first stage of the SP MDC prototype is generated on three identical helical surfaces which

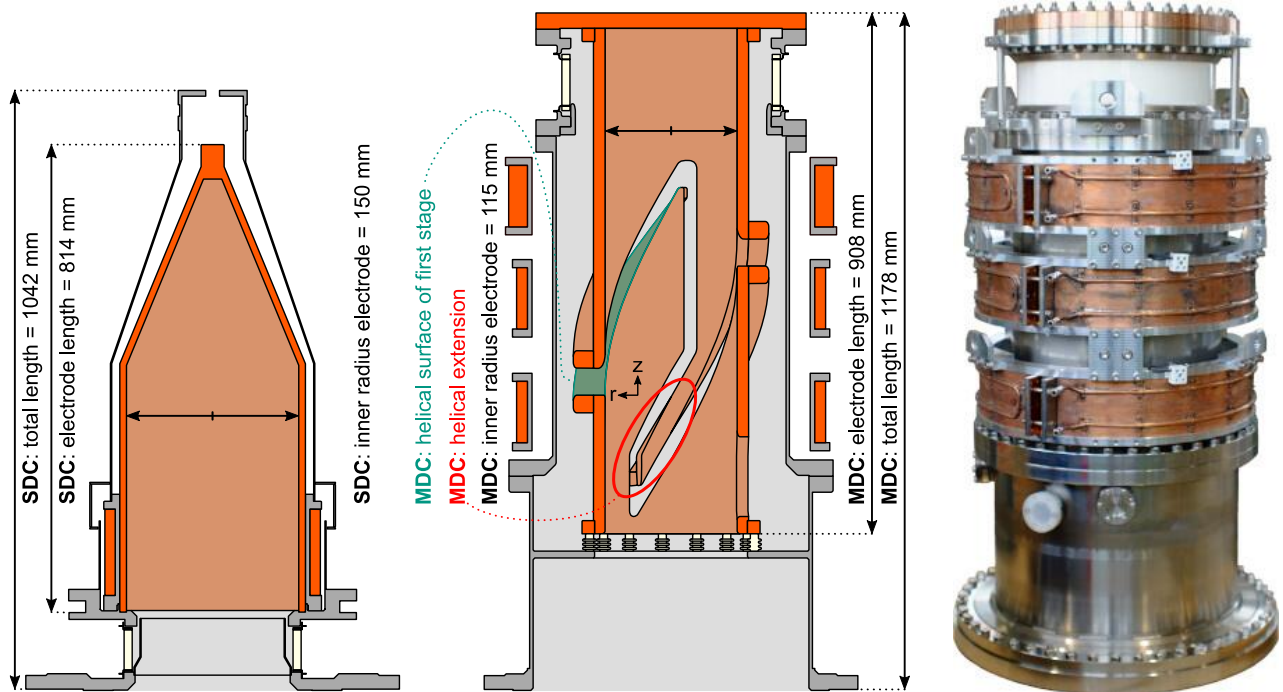


Fig. 2: Size comparison between the SP SDC and the SP MDC with a photo of the manufactured SP MDC prototype on the right. The fast spent electrons in the MDC are collected at the upper cylindrical section of the second stage. The slow spent electrons are collected at the three helical surfaces of the first stage (one marked in green).

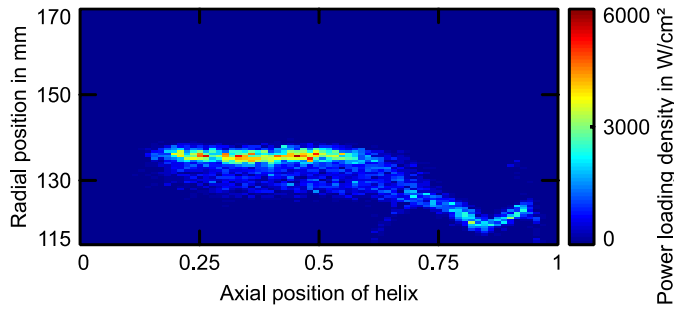


Fig. 3: Power loading density on first stage of the SP MDC. The helical surfaces are projected to a 2D plane with their radial and axial position.

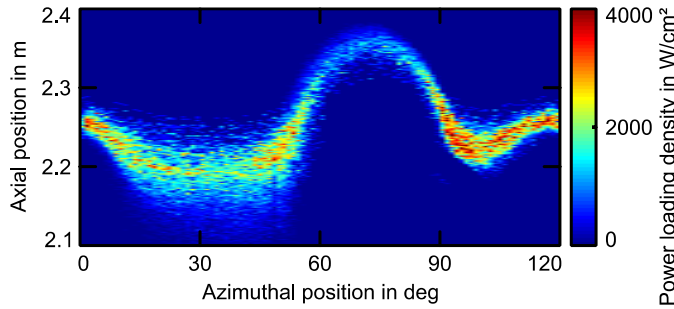


Fig. 4: Power loading density on second stage of the SP MDC.

are projected to one 2D plane and shown in Fig. 3. It should be mentioned that the thermal loading is concentrated on a thin line with a thickness of only a few millimeters from bottom to top of the helical surface. The radial position of electron collection is dependent on the strength of the $E \times B$ drift. The power loading density on the cylindrical surface of the second stage is shown in Fig. 4. Only a 120° segment is shown due to the symmetry condition of the triple helix design. The axial position of the thermal loading is azimuthally varied due to the different

directions of the radial electron drift caused by the E_ϕ component of the helical and straight cut as well as the helical extension at the bottom of the $E \times B$ region. The maximum power loading density on the first and second stage is below 6 kW/cm^2 and 4 kW/cm^2 , respectively. The maximum power loading density of the verified SP SDC for the 170 GHz 2 MW coaxial cavity gyrotron is at 6 kW/cm^2 with a depression potential of -35 kV . The total power deposition is significantly higher at 1580 kW in the SDC compared to 110 kW on the first stage and 750 kW on the second stage of the MDC prototype.

III. CONTINUOUS WAVE COLLECTORS

The most characteristic changes between a SP SDC and a CW SDC [19] is a larger size in radial and axial direction for a reduced overall power loading density as well as the implementation of a sweeping system for a reduced time averaged power loading density [20]. The main limitation of gyrotron collectors for longer pulse or CW operation are the cooling capabilities. Up to now, one of the most sophisticated and established cooling techniques for large objects like a high power gyrotron collector is the HyperVapotron cooling. The maximum acceptable time averaged power loading density of a slow cyclic loading in the order of 10 Hz at the inner collector wall is considered to 500 W/cm^2 for CW operation [21]. The collector size is significantly increased with the gyrotron output power, making it the largest component in a high power gyrotron. The inner collector radius of the European 1 MW CW gyrotron for ITER is at 225 mm whereas the inner collector radius of the CW SDC of the KIT 2 MW coaxial cavity gyrotron is at 300 mm, as shown in Fig. 5 on the left side. The inner collector radius for a 4 MW gyrotron with an SDC would be increased to 400 mm for identical material constraints [22, 23].

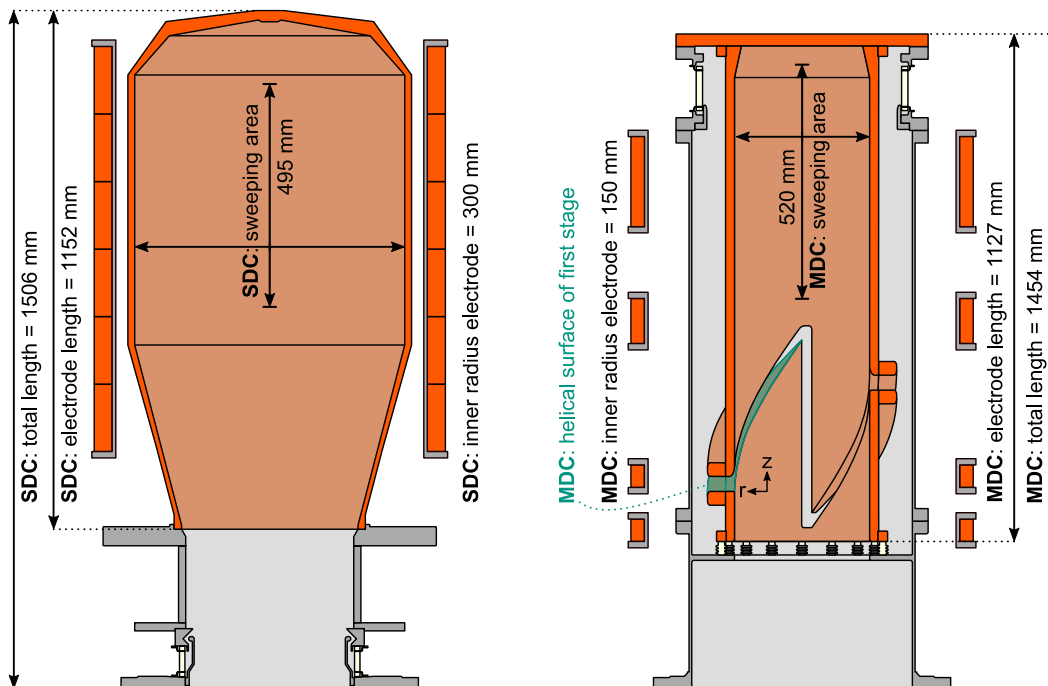


Fig. 5: Size comparison between the CW SDC and the CW MDC. The fast spent electrons in the MDC are collected at the upper cylindrical section of the second stage. The slow spent electrons are collected at the three helical surfaces of the first stage (one marked in green).

The same principle of an increased size of the collector stages is applied for the CW compatible MDC design approach [24]. The inner radius of the collector stages is increased from 115 mm of the SP MDC to 150 mm and the electron beam radius in the collector is raised from 98 mm to 127 mm. The initial axial position of the $E \times B$ region is moved to a higher axial position due to the increased beam radius and the identical magnetic field profile of the gyrotron magnet. The stages of an MDC system can be significantly reduced in size in comparison to a conventional SDC due to the reduced absolute power loading at the collector surface. A size comparison between the 2 MW CW SDC and CW MDC is shown in Fig. 5 including some of the key dimensions. The preliminary MDC design as shown here is an up-scaled version of the SP MDC. The design of the cooling system is not implemented at this state however, it is important to note that both cooling circuits must be set up independently of each other to avoid insulators of the cooling pipes inside the vacuum. It is planned to implement a HyperVapotron cooling for the cylindrical top section of the second stage and water-cooling channels under the helical surface of the first stage.

Additional collector coils are required for the homogenization of the magnetic field in the $E \times B$ region of the MDC system to achieve a constant electron beam radius. A summarized constant coil current of 37,800 ampere-turns is applied for the first conceptual design of a CW MDC. In addition, a summarized alternating current with a peak value of 10,500 ampere-turns is applied to the two upper coils for the magnetic field sweeping. The summarized alternating peak current of the six sweeping coils of the CW SDC is 10,800 ampere-turns. The axial length of the sweeping area is close to 500 mm for both collector designs.

IV. SWEEPING SYSTEMS FOR A CW MDC

The increased size in radial dimension is not sufficient for an acceptable power loading density at the first stage. A further decrease of the power loading density on the helical surface is possible by either a decreased absolute power on the first stage, or a sweeping system for the first stage. A combination of both approaches is also possible.

The only possibility for a sweeping system on the first stage is a variation of the radial position of the spent beam electrons on the helical surface. The final radial position is the sum of the beam radius in the collector plus the drift distance D , when no beam thickness is considered. A variation of the beam radius is not planned, due to the increased sensitivity to stray magnetic fields for a beam radius closer to the collector stage and a higher reflected current for a beam radius further away from the collector stage. A variation of the drift distance D is therefore the preferred option for a sweeping system on the first stage. The drift distance D is defined as:

$$D = \frac{2mv_0}{qB_{\parallel}} \tan \vartheta ,$$

for the simplified case of a planar electron drift [25]. The mass of the electron m , the charge of the electron q and the magnetic field parallel to the axis B_{\parallel} are constant. The angle ϑ between the electric and magnetic field in the collector is dependent on the geometry of the MDC and is therefore constant for a realistic system without moving parts. The velocity v_0 of the

spent electrons at the moment when they reach the $E \times B$ region is the only variable which can be swept. It can be increased reducing the deceleration potential at the collector entrance, or vice versa; while the potential of the second stage should not be changed to keep a high collector efficiency.

A variation of the absolute power collected at the first stage is the most critical factor when the collector potentials are varied in an MDC. The theoretical power fraction of the spent electron beam collected at the first stage without a reflected current versus the depression potentials as function of the applied potentials of the two collector stages is shown in Fig. 6. The voltage operation points with constant potential difference ΔU between both stages are represented by straight lines. The radial position at which the spent electron beam is collected at the first stage is directly related to the potential difference, as it is proportional to the electron drift. A strong change of the potential difference is required to sweep the electron beam. The absolute power loading on the first stage is reduced compared to the SP MDC. Four different operation points were chosen along the line of 40 kW of power on the first stage to present the idea of an $E \times B$ sweeping system. The highest depression potential on the first stage was limited to 35 kV as applied in the conventional SDC to avoid reflections at the collector entrance. The simulation results of the different operation points are summarized in Tab. 1. It should be mentioned that the absolute power loading on the first stage is in all cases higher than the theoretical value due to the collection of some electrons with higher initial kinetic energies. The absolute power loading on the second stage is only slightly influenced and is in a non-critical range. The collector efficiency is varied over time due to the change in the voltage operation point.

The power loadings on the first stage for different operation points are shown in Fig. 7. The power loadings are pushed to a larger radial position with increased potential difference

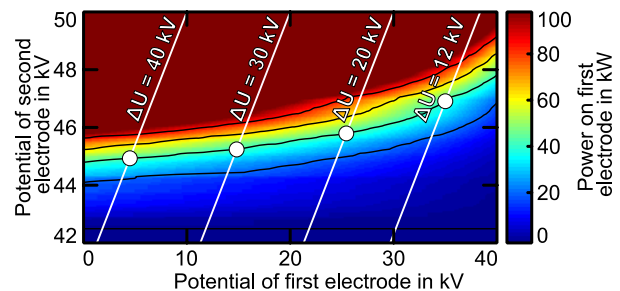


Fig. 6: Theoretical power loading on the first stage versus depression potentials of both collector stages.

Tab. 1: Simulation results for different operation points. The total gyrotron efficiency is calculated under the consideration of 35 % interaction efficiency and 10 % RF losses.

ΔU	40 kV	30 kV	20 kV	12 kV
Potential of first stage	-4.8 kV	-15.2 kV	-25.7 kV	-35 kV
Potential of second stage	-44.8 kV	-45.2 kV	-45.7 kV	-46.8 kV
Power loading on first stage	67 kW	44 kW	46 kW	46 kW
Reflected current	68 mA	107 mA	231 mA	518 mA
Collector efficiency	78.2 %	79.4 %	80.0 %	81.6 %
Total gyrotron efficiency	64.1 %	65.1 %	65.6 %	67.1 %

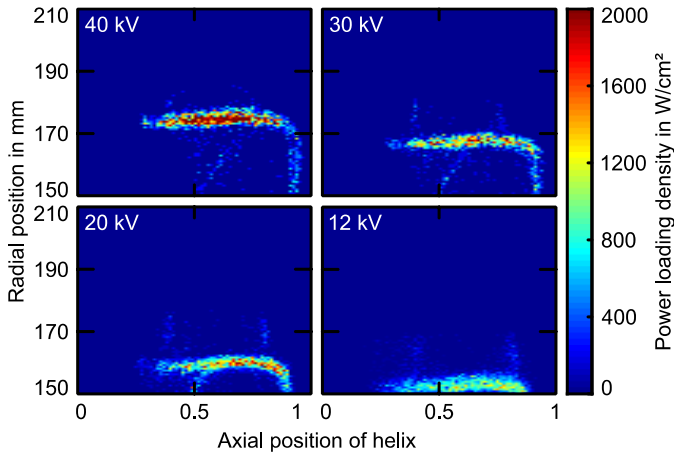


Fig. 7: Power loading density on the first stage of the CW MDC with $E \times B$ sweeping for different operation points. The helical surfaces are projected to a 2D plane with their radial and axial position.

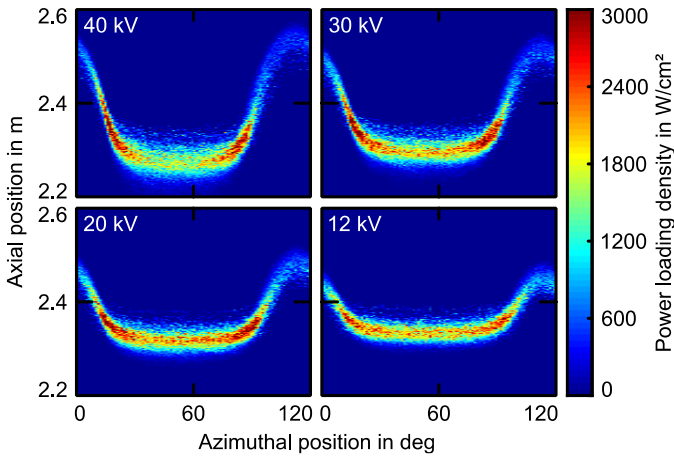


Fig. 8: Power loading density on the second stage of the CW MDC with $E \times B$ sweeping for different operation points.

between both stages due to the increased $E \times B$ drift. The reason for the increased reflected current for a potential difference of 12 kV is clearly visible by the close proximity of the power loading to the inner edge of the helical surface. The higher reflected current could be prevented by a higher minimal potential difference or a steeper helical cut between both stages. The power loadings on the second stage are varied in axial direction for different operation points and are shown in Fig. 8. The power loading at the azimuthal location of the helical cut is pushed to a lower axial position with increased potential difference and to a higher axial position at the azimuthal location of the straight cut. The power loading at the intermediate locations is not significantly influenced by the $E \times B$ sweeping. The power loadings of the first and second stage with identical voltage operation points are calculated together in the same simulation.

The time averaged power loadings on the first and second stage are shown in the top of Fig. 9 and Fig. 10, respectively. The power loading is distributed effectively on the helical surface and significantly improved on most of the cylindrical surface of the second stage.

Traditional magnetic field sweeping systems are limited in the sweeping frequency due to high eddy currents which are induced in the collector wall. The $E \times B$ sweeping is not limited

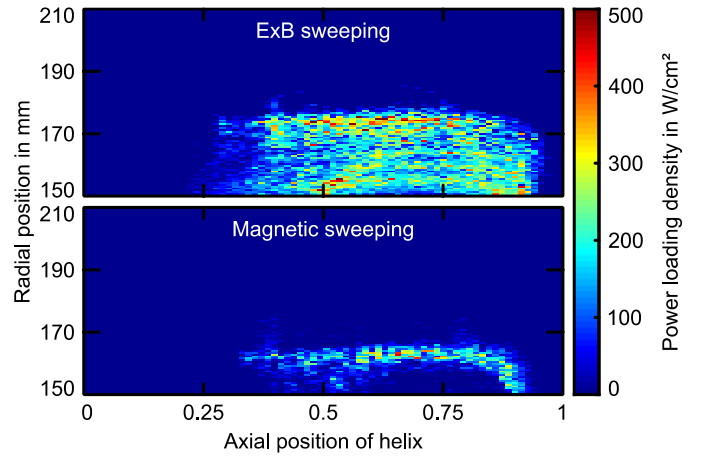


Fig. 9: Time averaged power loading density on the first stage of the CW MDC with $E \times B$ sweeping (top) and magnetic field sweeping (bottom). The helical surfaces are projected to a 2D plane with their radial and axial position.

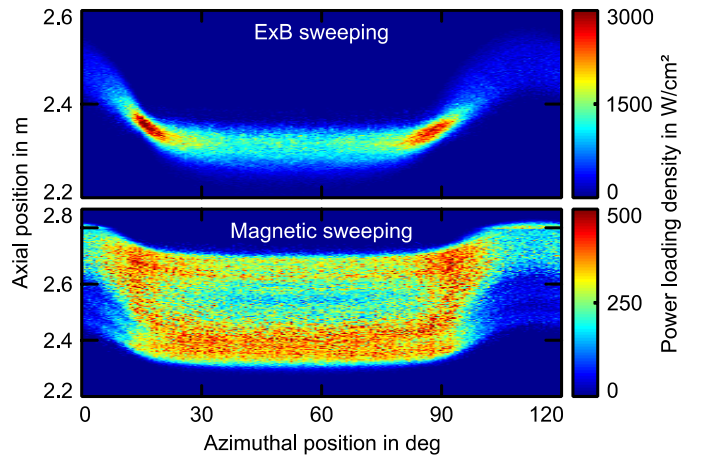


Fig. 10: Time averaged power loading density on the second stage of the CW MDC for the $E \times B$ sweeping (top) and magnetic field sweeping (bottom).

to such low sweeping frequencies. The cyclic fatigue in the collector could be decreased by a higher sweeping frequency which could significantly improve the maximum acceptable power loading density. However, those expectations are exceeded in this design with the maximum power loading density of up to 3 kW/cm² at some points of the second stage in case of a pure $E \times B$ sweeping.

Another possibility for the operation of a CW MDC is a fixed voltage operation point with a small absolute power loading on the first stage and an axial magnetic field sweeping system for the second stage. A depression potential of -25 kV for the first stage and -44 kV for the second stage were chosen. A collector efficiency of 78.1 %, a total gyrotron efficiency of 64.0 %, a reflected current below 65 mA and a power loading of 11 kW on the first stage were achieved in simulation, independent of the phase of the sweeping cycle. The trajectory simulations were performed in steady state for different time steps and combined in post-processing. No eddy currents are considered in the system and an advanced sweeping function was chosen. The time averaged power loadings on the first and second stage are shown in the bottom of Fig. 9 and Fig. 10, respectively. The thermal loading on the helical surface of the first stage is not influenced by the magnetic field sweeping system of the second

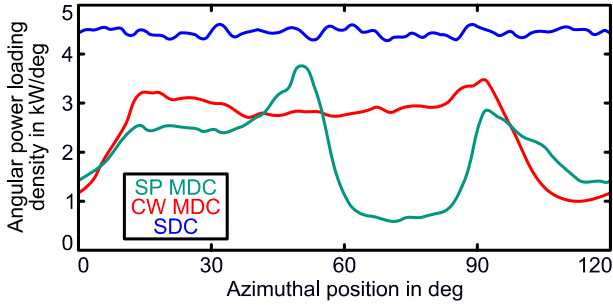


Fig. 11: Angular power loading density for an SDC, the SP MDC and CW MDC with magnetic field sweeping.

stage. The goal of a maximum power loading density of under 500 W/cm² without secondary electron emission was achieved for this design. The following parts of this work will be concentrated to the CW MDC with exclusive magnetic field sweeping due to the acceptable loading densities on both stages and the lower demands on the gyrotron power supply compared to the CW MDC with $E \times B$ sweeping system.

The instantaneous maximum power loading density of the CW SDC and CW MDC with magnetic field sweeping is at 3.7 kW/cm² at the lower turning point of the sweep cycle [26]. The high instantaneous power loading density in the MDC is limited to in total six small areas at the azimuthal position of the transition between the straight and helical cut. It is reduced to less than 3.0 kW/cm² at the azimuthal position of the helical cut and to less than 1.3 kW/cm² at the azimuthal position of the straight cut. The power loading density in the CW SDC is independent on the azimuthal position. The maximum power loading density in the MDC is varied in azimuthal direction due to different beam thicknesses caused by the $E \times B$ drift and variations in the angular line density. The line density of the thermal loading in azimuthal direction is in direct correlation to the absolute power that is absorbed in an angular segment of the cylindrical collector wall and is shown in Fig. 11. The azimuthal variation of the thermal loading is created by an azimuthal electron drift due to radial electric field components E_r near the edges of the cut between the collector stages. The

azimuthal electron drift is strongest in the area of the straight cut (between 100° to 120° for the CW MDC) and is most noticeable due to a drift direction away from the cut and therefore a reduced thermal loading at this position. The angular line density for an SDC is constant due to the symmetry condition and is independent on the collector geometry. The average angular line density is correlated with the efficiency of the collector and is different for all three collector systems.

V. THERMAL EXPANSION FOR CW MDC

The thermal expansion in general is dependent on the temperature and temperature differences in a material. The temperature profile on the inner collector wall is in direct correlation to the thermal loading. In this section, the influence of the azimuthally varied thermal loading in the CW MDC to the thermal expansion of the second collector stage with a complex geometry is studied. The thermal simulations for a representation of a water cooling were performed in ANSYS with an imported power loading profile, a 3D geometry, a heat transfer coefficient of 8000 W/(m²·K) and an ambient temperature of 19°C. The utilized heat transfer coefficient is in the range for a cooling with water-forced convection [27] and is a preliminary investigation for a worst-case scenario. The heat transfer coefficient for a HyperVapotron cooling is in the range of 8500 to 23000 W/(m²·K) in combination with a larger surface [21]. The second collector stage is fixed at the top plate as shown in Fig. 5. The steady state temperature at the inner collector wall is shown in Fig. 12 (a) and is in correlation to the power loading as expected. The thermal expansion in radial direction is shown in Fig. 12 (b) and the deformation at the cylindrical top section is only slightly varied. The absolute value of deformation at the cylindrical top section should be uncritical as it is proportional to the collector size. The maximum power load density and thus the temperature and relative deformation should be identical to the validated CW SDC. However, the deformation at the lower part of the helical section is more critical, as a correct placement for a constant gap between both electrodes is required to achieve a well-

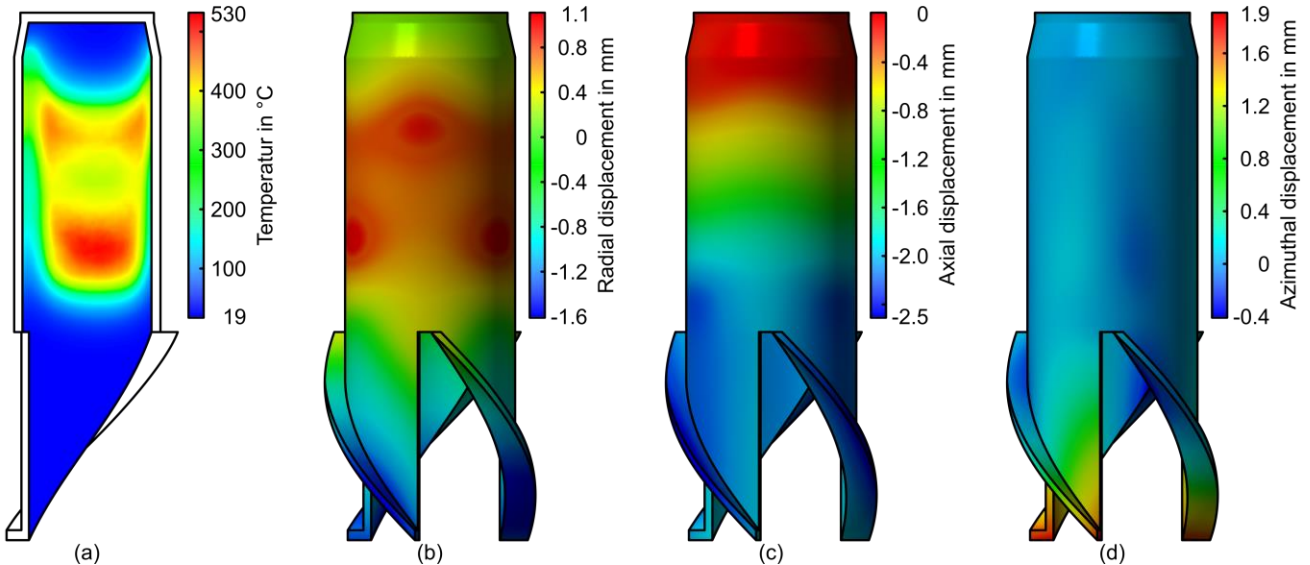


Fig. 12: Temperature (a) and thermal expansion in radial (b), axial (c) and azimuthal (d) direction of the CW MDC.

defined $E \times B$ drift. The same arguments also apply to the axial and azimuthal thermal expansion as shown in Fig 12 (c) and (d), respectively.

The thermal deformation at the lower part of the second collector stage could be significantly improved by a different mounting method as the fixation at the top plate is not ideal. A mount directly above the $E \times B$ region should be more optimal since the lower part of the second collector stage is not heated. The thermal expansion has to be considered for future more realistic mechanical designs of an $E \times B$ drift CW MDC.

VI. CONCLUSION

The SP MDC prototype for a 2 MW 170 GHz coaxial-cavity gyrotron was presented in comparison to a conventional SP SDC. The main limitation in the maximum pulse length of a SP collector is a high power loading density at the inner surface of the collector stage. A pure increase in size is not sufficient for an acceptable maximum power loading density. Two different sweeping concepts were presented to distribute the power loading to a larger surface and the importance of the voltage operation point was mentioned. A comparison in size, sweeping system and maximum power loading density of the up-scaled CW MDC to a CW SDC of a 2 MW gyrotron was given. The influence of the thermal expansion in a CW MDC was discussed. No principle showstoppers were found for the CW MDC in power loading density or mechanical deformation, provided they are considered in future design iterations.

REFERENCES

- [1] K. Sakamoto, M. Tsuneoka, A. Kasugai, T. Imai, T. Kariya, K. Hayashi, Y. Mitsunaka, "Major improvement of gyrotron efficiency with beam energy recovery," *Phys. Rev. Lett.*, vol. 73, no. 26, pp. 3532–3535, December 1994, doi: 10.1103/PhysRevLett.73.3532.
- [2] B. Piosczyk, C.T. Iatrou, G. Dammertz, M. Thumm, "Single-stage depressed collectors for gyrotrons," *IEEE Trans. on Plasma Sci.*, vol. 24, no. 3, pp. 579–585, June 1996, doi: 10.1109/27.532940.
- [3] M.Y. Glyavin, A.N. Kuftin, N.P. Venediktov, V.E. Zapevalov, "Experimental investigation of a 110 GHz/1 MW gyrotron with the one-step depressed collector," *Int. J. Infrared Millimeter Waves*, vol. 18, no. 11, pp. 2129–2136, November 1997, doi: 10.1007/BF02678255.
- [4] I.Gr. Pagonakis, J.-P. Hogge, S. Alberti, K.A. Avramidis, J.L. Vomvoridis, "A new concept for the collection of an electron beam configured by an externally applied axial magnetic field," *IEEE Trans. on Plasma Sci.*, vol. 36, no. 2, pp. 469–480, April 2008, doi: 10.1109/TPS.2008.917943.
- [5] B. Ell, I.Gr. Pagonakis, C. Wu, M. Thumm, J. Jelonnek, "Coaxial multistage depressed collector design for high power gyrotrons based on $E \times B$ concept," *Phys. of Plasmas*, vol. 26, 113107, pp. 1–8, November 2019, doi: 10.1063/1.5118338.
- [6] C. Wu, I.Gr. Pagonakis, S. Illy, G. Gantenbein, M. Thumm, J. Jelonnek, "Comparison between controlled non-adiabatic and $E \times B$ concepts for gyrotron multistage depressed collectors," *EPJ Web Conf.*, vol. 149, 04005, pp. 1–2, August 2017, doi: 10.1051/epjconf/201714904005.
- [7] V.N. Manuilov, M.V. Morozkin, O.I. Luksha, M.Yu Glyavin, "Gyrotron collector systems: Types and capabilities," *Infrared Physics & Technology*, vol. 91, pp. 46–54, June 2018, doi: 10.1016/j.infrared.2018.03.024.
- [8] M. Glyavin, V. Manuilov, M. Morozkin, "Two-stage energy recovery system for DEMO gyrotron," in 43rd Int. Conf. on Infrared, Millimeter, and Terahertz Waves (IRMMW-THz), pp. 1–2, October 2018, doi: 10.1109/IRMMW-THz.2018.8510139.
- [9] O.I. Louksha, P.A. Trofimov, "A method of electron separation for multistep recuperation systems in gyrotrons," *Tech. Phys. Lett.*, vol. 41, pp. 884–886, September 2015, doi: 10.1134/S1063785015090230.
- [10] I.Gr. Pagonakis, C. Wu, S. Illy, J. Jelonnek, "Multistage depressed collector conceptual design for thin magnetically confined electron beams," *Phys. of Plasmas*, vol. 23, pp. 1–8, 043114, April 2016, doi: 10.1063/1.4947565.
- [11] C. Wu, I.Gr. Pagonakis, S. Illy, M. Thumm, G. Gantenbein, J. Jelonnek, "Preliminary studies on multistage depressed collectors for fusion gyrotrons," in German Microwave Conf. (GeMic), pp. 365–368, May 2016, doi: 10.1109/GEMIC.2016.7461632.
- [12] C. Wu, I.Gr. Pagonakis, G. Gantenbein, S. Illy, M. Thumm, J. Jelonnek, "Conceptual designs of $E \times B$ multistage depressed collectors for gyrotrons," *Phys. of Plasmas*, vol. 24, pp. 1–8, 043102, March 2017, doi: 10.1063/1.4979291.
- [13] C. Wu, I.Gr. Pagonakis, K.A. Avramidis, G. Gantenbein, S. Illy, M. Thumm, J. Jelonnek, "Gyrotron multistage depressed collector based on $E \times B$ drift concept using azimuthal electric field. I. Basic design," *Phys. of Plasmas*, vol. 25, pp. 1–10, 033108, March 2018, doi: 10.1063/1.5016296.
- [14] C. Wu, I.Gr. Pagonakis, D. Albert, K.A. Avramidis, G. Gantenbein, S. Illy, M. Thumm, J. Jelonnek, "Gyrotron multistage depressed collector based on $E \times B$ drift concept using azimuthal electric field. II: Upgraded designs," *Phys. of Plasmas*, vol. 26, pp. 1–6, 013108, January 2019, doi: 10.1063/1.5078861.
- [15] B. Ell, I.Gr. Pagonakis, C. Wu, D. Albert, G. Gantenbein, S. Illy, T. Kobarg, T. Rzesnicki, M. Thumm, J. Jelonnek, "Mechanical design study for gyrotron $E \times B$ drift two-stage depressed collector," in 21st Int. Vacuum Electronics Conf. (IVEC), pp. 187–188, August 2021, doi: 10.1109/IVEC45766.2020.9520565.
- [16] B. Ell, I.Gr. Pagonakis, C. Wu, G. Gantenbein, S. Illy, T. Rzesnicki, S. Stanculovic, M. Thumm, J. Weggen, J. Jelonnek, "Mechanical design of the short pulse $E \times B$ drift two-stage depressed collector prototype for high power gyrotron," in 22nd Int. Vacuum Electronics Conf. (IVEC), pp. 1–2, March 2022, doi: 10.1109/IVEC51707.2021.9722425.
- [17] T. Rzesnicki, B. Piosczyk, S. Kern, S. Illy, J. Jin, A. Samartsev, A. Schlaich, M. Thumm, "2.2-MW record power of the 170-GHz european pre-prototype coaxial-cavity gyrotron for ITER," *IEEE Trans. on Plasma Sci.*, vol. 38, no. 6, pp. 1141–1149, June 2010, doi: 10.1109/TPS.2010.2040842.
- [18] B. Lyu, "Thermal investigation and lifetime estimation for the design improvement of a 2 MW fusion gyrotron collector," Master's thesis, Karlsruhe Institute of Technology, Karlsruhe, Germany, July 2020.
- [19] G. Dammertz, S. Illy, B. Piosczyk, M. Schmid, D. Bariou, "Collector sweeping systems for high power gyrotrons," *Joint 30th Int. Conf. on Infrared and Millimeter Waves and 13th Int. Conf. on Terahertz Electronics (IRMMW-THz)*, vol. 1, pp. 293–294, January 2006, doi: 10.1109/ICIMW.2005.1572524.
- [20] M. Schmid, S. Illy, G. Dammertz, V. Erckmann, M. Thumm, "Transverse field collector sweep system for high power CW gyrotrons," *Fusion Engineering and Design*, vol. 82, no. 5–14, pp. 744–750, October 2007, doi: 10.1016/j.fusengdes.2007.06.008.
- [21] D. Bariou, C. Lievin, "Extract from RT 5307 design report ITER 170 GHz Gyrotron," *Tech. Rep. EFDA-03/960*, December 2007.
- [22] M. Beringer, "Design studies towards a 4 MW 170 GHz coaxial-cavity gyrotron," Doctoral dissertation, Karlsruhe Institute of Technology, Karlsruhe, Germany, 2011, doi: 10.5445/KSP/1000022514
- [23] M.H. Beringer, S. Kern, M. Thumm, "Mode selection and coaxial cavity design for a 4 MW 170 GHz gyrotron including thermal aspects," *IEEE Trans. on Plasma Sci.*, vol. 41, no. 4, pp. 853–861, April 2013, doi: 10.1109/TPS.2013.2251870.
- [24] B. Ell, C. Wu, G. Gantenbein, S. Illy, I.Gr. Pagonakis, T. Rzesnicki, S. Stanculovic, M. Thumm, J. Weggen, J. Jelonnek, "Design of a two-stage depressed collector for continuous wave operation of MW-class gyrotrons," in 23rd Int. Vacuum Electronics Conf. (IVEC), submitted.
- [25] C. Wu, "Conceptual studies of multistage depressed collectors for gyrotrons," Doctoral dissertation, Karlsruhe Institute of Technology, Karlsruhe, Germany, 2019, doi: 10.5445/KSP/1000094598.
- [26] S. Illy, B. Piosczyk, "Simulating the effect of secondary emission in the collector of high power CW gyrotrons," in 35th IEEE Int. Conf. on Plasma Sci. (ICOPS), p. 1, August 2008, doi: 10.1109/PLASMA.2008.4591131.
- [27] W.L. Cheng, W.W. Zhang, H. Chen, L. Hu, "Spray cooling and flash evaporation cooling: The current development and application," *Renewable and Sustainable Energy Reviews*, vol. 55, pp. 614–628, March 2016, doi: 10.1016/j.rser.2015.11.014.